RSC Advances

ROYAL SOCIETY OF CHEMISTRY

www.rsc.org/advances

A novel composite MIL-101@GO based on MIL-101(Cr) and graphite oxide (GO) shows high adsorption capacities and excellent adsorption/desorption performance for a series of *n*-alkanes.

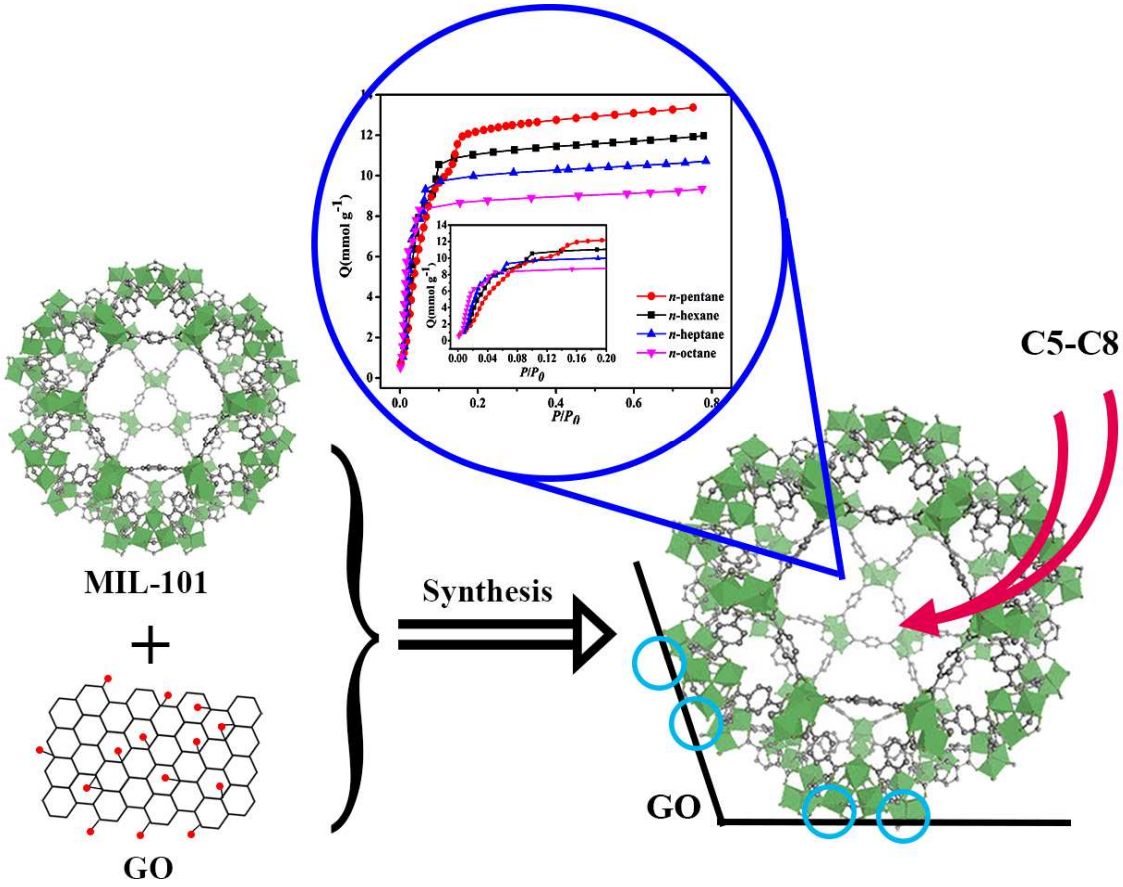

Adsorption performance of composite MIL-101(Cr)/graphite oxide for a series of *n*-alkanes

Xuejiao Sun, Yujie Li, Hongxia Xi, Qibin Xia*,

ABSTRACT:

Adsorption performance of composite MIL-101@GO for a series of linear long chain alkanes (from *n*-pentane to *n*-octane) was first investigated. The composite MIL-101@GO based on MIL-101(Cr) and graphite oxide (GO) was prepared, characterized and tested for adsorption and desorption of *n*-alkanes. Isotherms of a series of *n*-alkanes on MIL-101@GO were measured. Temperature-programmed desorption (TPD) experiments were conducted to estimate desorption activation energies of *n*-alkanes on MIL-101@GO. Results showed that the adsorption capacities of *n*-alkanes on MIL-101@GO increased with the hydrocarbon chain length at region of low pressure, while the trend was reversed at region of high pressure. The adsorption capacities of *n*-alkanes on MIL-101@GO were about 1.6-11 times higher than those of conventional activated carbons and the zeolites. The isotherms of *n*-alkanes could be fitted favorably by the Langmuir-Freundlich equation. Desorption activation energy increased linearly with the carbon number of *n*-alkanes. Consecutive cycle experiments of adsorption-desorption showed the isotherms of *n*-octane in all five cycles were nearly overlapping, suggesting that MIL-101@GO had excellent reversibility of *n*-alkane adsorption.

Keywords: Adsorption; MOF; Graphite oxide; Composite; MIL-101; Alkanes

1. Introduction

Gasoline is a transparent, petroleum-derived liquid that is widely used as a fuel, diluent, finishing agent, and industrial solvent. It consists of hydrocarbons with between 4 and 12 carbon atoms per molecule (commonly referred to as C4-C12), including alkanes, cycloalkanes, alkenes, and aromatics.[1] Because of its strong volatility, a large amount of gasoline vapor is emitted from tanks into the atmosphere in the operation processes (*e.g.*, storage, transportation, loading, and unloading) used in oil refineries, petrochemical factories, oil depots, oil terminals, and gas stations.[2-3] These emissions lead to a series of direct or indirect harmful effects, such as energy resource wastage and significant economic loss, increased risk of fire accidents, increased environmental pollution and

School of Chemistry and Chemical Engineering, South China University of Technology, Guangzhou 510640, PR China. E-mail: qbxia@scut.edu.cn

damage to human health.[4-5] Therefore, development of advanced technologies for efficient recovery and removal of gasoline vapor is of great significance in both environmental and energy sciences. Various technologies have been introduced for controlling evaporative emission and the gasoline recovery, such as adsorption, condensation, and membrane separation.[6-8] Adsorption is one of the most effective techniques for hydrocarbon removal because of its high energy efficiency and low operating cost. [9, 10]

The core of adsorption technology is an adsorbent. Development of an advanced adsorbent with high adsorption capacity is crucial. Traditional porous materials such as activated carbon and zeolites showed low adsorption capacities toward hydrocarbons.[11, 12] Recently, metal-organic frameworks (MOFs), as a new family of crystalline adsorbents, have attracted more and more attention due to their ultrahigh specific area, tunable pore structures and surface functionality,[13-19] which makes them have potential application for adsorption of gaseous pollutants, especially hydrocarbons. For example, Zhao and co-workers[20, 21] reported that MIL-101 had very high adsorption capacities of 16.5 and 10.9 mmol g^{-1} for benzene and p-xylene at 288 K, respectively. Shi et al.[22] tested the adsorption of ethyl acetate on MIL-101 and reported the uptake of ethyl acetate was up to 10.5 mmol g^{-1} at 288 K and 54 mbar. These adsorption capacities are much higher than those of conventional adsorbents such as activated carbons and zeolites. Moreover, adsorption of *n*-alkanes on MOFs such as ZIF-8,[23] MIL-47,[24, 25]MIL-100(Cr), MIL-101(Cr),[26] MIL-53(Cr),[27] and a series of flexible MIL-88(Fe) structures[28] was reported. Trung et al.[27] studied the adsorption of *n*-alkanes on a flexible MIL-53(Cr) and reported that its maximum *n*-hexane uptake was 3 mmol g^{-1} at 313 K. Ramsahye et al.[28] reported that the maximum adsorption capacities of MIL-88A for *n*-pentane and *n*-hexane were 1.2 and 0.64 mmol g^{-1} at 303 K, respectively. Huang et al.[29] reported that the *n*-hexane uptake of the MIL-101 was about 0.07 mmol g^{-1} at 303 K and 2.25 mbar. In addition, some investigators also tried to further improve the adsorption performance of MOFs toward gaseous pollutants by means of recombination of MOFs and inorganic species (such as carbon nanotube, graphite oxide, and activated carbon) carbon materials.[30-32] For example, Bandosz and coworkers[26, 33] prepared composites of MOFs and graphite oxide (GO) such as MOF-5/GO and HKUST-1/GO. Their results showed that the adsorption properties of NH_3, NO_2, and H_2S on these composites MOF/GO were significantly improved in comparison with that of their parent MOF. Kumar et al.[34] prepared hybrid nanocomposites based on graphene oxide and ZIF-8, and reported the enhanced CO_2 adsorption capacity of the composites. MIL-101 is an attractive candidate for the adsorption of gas due to its extra-high specific surface area, pore volume, outstanding thermal and chemical stability.[35, 36] Liu et al.[37] tried to synthesize the MIL-101@GO composites. Unfortunately, the incorporation of large amounts of GO resulted in a pronounced decrease in the porosity and specific surface area of the composites, which could be attributed to the unsuitable synthesis conditions

of the composites. Ahmed et al.[38] also prepared the MIL-101@GO composites and reported the improvement in adsorption capacity for nitrogen-containing compounds of model fuels compared to virgin MIL-101. Recently, our group synthesized the composites of MIL-101 and GO as well as graphene oxide (GrO), and it was found that the composites had higher adsorption capacities for both polar acetone molecules and non-polar *n*-hexane molecules than its parent MIL-101,[39, 40] which was attributed to the fact that introduction of a small fraction of GrO to MIL-101 crystals significantly resulted in an increase in surface area and dispersive forces towards gas molecules of the composites. *n*-Alkanes (C5-C8) are main components of gasoline vapors, which are classified as highly flammable (F), harmful (Xn) and dangerous for the environment (N). It is possible that this novel composite material will have excellent adsorption performance for a series of *n*-alkanes. Therefore, the adsorption behavior of these *n*-alkanes is worthy of studying, which has not been reported so far.

The objective of this work is to investigate the adsorption performance of a novel composite MIL-101@GO for a series of *n*-alkanes (C5-C8). The adsorption isotherms of *n*-alkanes on MIL-101@GO sample were measured by volumetric method. Temperature program desorption (TPD) experiments were conducted to evaluate the interaction between *n*-alkanes and MIL-101@GO. Consecutive adsorption-desorption cycles were also performed to examine the reversibility of *n*-alkanes adsorption on MIL-101@GO. The effects of properties of *n*-alkanes on their adsorption on MIL-101@GO would be discussed and reported here.

2. Experimental

2.1. Materials

The MIL-101 and MIL-101@GO used in this study were synthesized via hydrothermal method. The GO amount added in the preparation of the composite MIL-101@GO was 5 wt% of the initial material weight. Detailed descriptions of the synthesis and characterization of MIL-101 and MIL-101@GO were given in Supporting Information and reference[40]. BET surface area of MIL-101 and MIL-101@GO were obtained as 2936 and 3421 $m^2 g^{-1}$, respectively. The *n*-alkanes (A.R.) were purchased from Guangdong Guanghua Sci-Tech Co. Ltd (China).

2.2. Adsorption experiments

The vapor-phase adsorptions of *n*-alkanes (from *n*-pentane to *n*-octane) were performed at 298 K on a volumetric adsorption apparatus, i.e., 3Flex Surface Characterization Analyzer (Micromeritics Instrument Corporation, USA). The vapor generation system included a stainless steel chamber with a hard seal, manual cutoff valve to be attached in place of the Psat tube, and a heating mantle to control the temperature of the chamber

at an operator-specified temperature between ambient and 316 K. The constant adsorption temperature was achieved by putting sample cell into circulating water bath. The sample was weighed about 40 mg for each run. The initial outgassing process for each sample was carried out at 423 K under vacuum overnight.

2.3. Temperature programmed desorption experiments

In order to estimate desorption activation energies of *n*-alkanes on the MIL-101@GO sample, TPD experiments were carried out on gas chromatography workstation (GC-9560, Shanghai Wuhao, China) with an accuracy of 0.1K for measurement of temperature. TPD experiments were conducted at different heating rates from 4 to 8 K min^{-1}. For each run, the samples with adsorbed *n*-alkane vapor were packed in a stainless steel reaction tube with inner diameter of 0.3 cm and packed length of about 0.5 cm. The stainless tube was placed in a reaction furnace and heated in the high-purity N_2 flow at a constant flow rate of 30 mL min^{-1}. The desorbed *n*-alkanes were measured on line by GC-9560 chromatograph with a flame ionization detector at the outlet of the reaction tube and effluent curves (TPD curves) were recorded. Repeated tests have been run to confirm the reproducibility of data. The relative standard deviation of peak temperature is below 0.15%, showing good repetitiveness.

3. Results and discussion

3.1. Adsorption isotherms of n-alkanes

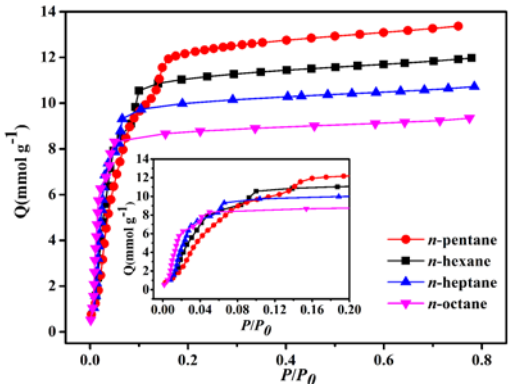

Fig. 1 Adsorption isotherms of *n*-alkanes on MIL-101@GO at 298 K

Fig. 1 shows the isotherms of *n*-alkanes C5-C8 on MIL-101@GO composite. It was observed that the adsorption capacities of *n*-alkanes on MIL-101@GO increased with the hydrocarbon chain length at region of low pressure, whereas the trend was reversed at region of high pressure. That is to say, at region of low pressure the adsorption capacities of *n*-alkanes C5-C8 on MIL-101@GO followed the order: C8 > C7 > C6 > C5, whereas at region of high pressure the adsorption capacities of *n*-alkanes C5-C8 on MIL-101@GO followed the order: C5 > C6 > C7 > C8. The two different trends are related to the physical properties of *n*-alkanes and their adsorption

mechanism on MIL-101@GO in the region of low and high pressure.

Table 1 Physical properties[41-43] and the maximum adsorption capacities of selected *n*-alkanes on MIL-101@GO.

Adsorbates	Polarizability×10^{25} (cm^3)	Molecular cross-sectional area (nm^2)	Molecular length (Å)	Q_a (mmol g^{-1})
n-Pentane（C5）	99.9	0.45	9.101	13.4
n-Hexane（C6）	119	0.51	10.344	11.9
n-Heptane（C7）	136.1	0.573	11.589	10.7
n-Octane（C8）	159	0.61	12.833	9.3

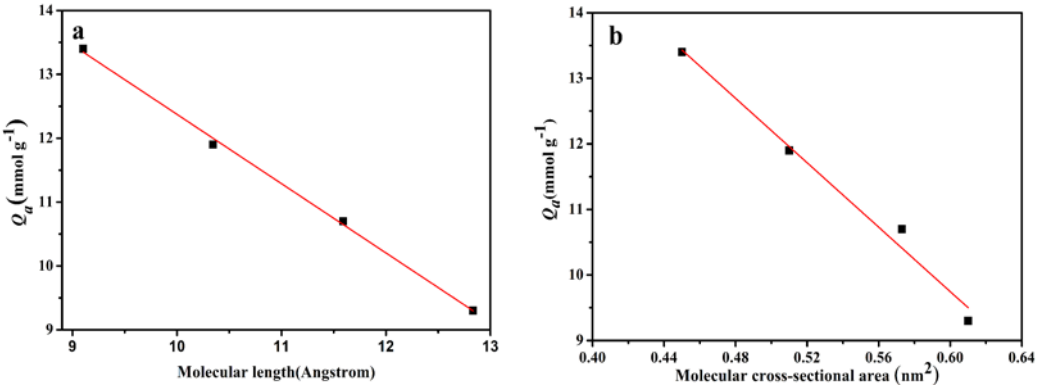

Fig. 2 Adsorption capacities of *n*-alkanes on MIL-101@GO as functions of (a) their molecular length and (b) cross-sectional area

Table 1 lists the physical properties[41-43] and the maximum adsorption capacities (Q_a) of selected *n*-alkanes on MIL-101@GO. It indicated that when *n*-alkane chain was elongated by a single -CH_2- group, its polarizability increased, and its molecular cross-sectional area and length increased. Thus, the molecule sizes of *n*-alkanes followed the order: C8 > C7 > C6 > C5. At region of low pressure, mono-adsorption is dominant. That is to say, it is dominated by the interaction between *n*-alkane and the surfaces of MIL-101@GO. Generally speaking, the larger the molecule size, the stronger the attraction forces acting on the molecule from the surface force field on the surrounding walls was for a porous material with fixed pore size and volume. As a result, *n*-alkanes with larger molecule size could have higher adsorption capacity, and thus the adsorption capacity of MIL-101@GO followed the order: C8 > C7 > C6 > C5. On the other hand, at region of high pressure, multilayer adsorption or pore filling would happen. Therefore, for a porous material with fixed pore size and volume, the larger the molecule size of *n*-alkanes was, the less the amounts of *n*-alkanes adsorbed within the pores of the adsorbent became due to its limited pore volume. As a consequence of that, the maximum adsorption capacities (Q_a) of MIL-101@GO for *n*-alkanes followed the order: C5 > C6 > C7 > C8, which were 13.4, 11.9, 10.7 and 9.3 mmol g^{-1}, as shown in

Table 1. Fig. 2 shows the plots of Q_a of *n*-alkanes in high pressure region versus their molecular length and cross-sectional area. It shows that the maximum adsorption capacities of *n*-alkanes decrease linearly with their molecular length and cross-sectional area.

It is also noticed that the isotherms exhibit slight sub-steps (inset Fig. 1) at low relative pressure which is mainly attributed to the filling of the two types of cages.[35] However, the sub-steps shift to the lower relative pressures as the alkyl chain length of *n*-alkanes increases. The relative pressure scale could be related to the free enthalpy of the vapor phase in equilibrium with the adsorbed phase. Therefore, it can be deduced that shorter *n*-alkanes require more energy to enter the small cavities of MIL-101@GO as compared to longer *n*-alkanes.[44] It could be suggested that the interaction between *n*-alkane and MIL-101@GO composite is much stronger as the alkyl chain length of *n*-alkanes increases. This is consistent with previous conclusion and will be further confirmed by TPD experiments in the next section.

Table 2 Adsorption capacities of the prepared composite and some other adsorbents for selected *n*-alkanes reported from the literature.

Adsorbates	Adsorbents	BET surface area (m^2 g^{-1})	Q_a (mmol g^{-1})	Temperature (K)	Ref
n-Pentane	CMK-3	1448	8.6	298	45
	SBA-15	829	6.9	298	45
	MCM-48	1126	8.2	298	45
	MIL-101	2936	10.7	298	present work
	MIL-101@GO	3421	13.4	298	present work
n-Hexane	activated carbon BPL	923	3.6	295	46
	hydrophobic zeolite Y	692	2.3	295	46
	ZSM-5	-	1.1	303	12
	MIL-101	2936	9.5	298	present work
	MIL-101@GO	3421	11.9	298	present work
n-Heptane	MCM-48	1300	6	294	47
	UL-ZSM5-100-6	780	2.9	303	48
	MIL-101	2936	8.5	298	present work
	MIL-101@GO	3421	10.7	298	present work
n-Octane	BAX950	-	5.2	298	49
	HZSM-5(3)	373	2.3	293	50
	MIL-101	2936	7.2	298	present work
	MIL-101@GO	3421	9.3	298	present work

In addition, MIL-101@GO composite also exhibits higher adsorption capacities of *n*-alkanes C5-C8 than the

parent MIL-101 (Fig. S3). For further comparison, Table 2 lists the *n*-alkanes adsorption capacities of some adsorbents reported by some investigators. It indicated that the *n*-alkanes adsorption capacities of MIL-101@GO increased by 25% -29% in comparison with that of the MIL-101, and were much higher than those of conventional adsorbents, which were about 1.6-11 times higher than that on the activated carbon and zeolites at similar conditions. Therefore, the MIL-101@GO is a promising adsorbent for adsorption of *n*-alkanes.

The Langmuir-Freundlich (L-F) equation is applied to fit the experimental isotherm data of *n*-alkanes in order to describe quantitatively relationship between amounts adsorbed and partial pressure of *n*-alkanes, which is very important or necessary to establish mathematical model for an adsorption process. Although Langmuir-Freundlich equation is not the model based on mechanism, it has widely been used as a semi-empirical equation to fit experimental isotherm or describe relationship between the adsorbed amounts and partial pressure of an adsorbate. The L-F equation can be expressed as[22]

$$Q = \frac{Q_{max} K P^{1/n}}{1 + K P^{1/n}} \quad (1)$$

where Q is the amount adsorbed in equilibrium with the concentration of adsorbate in gas phase (mmol g^{-1}), Q_{max} is the maximum adsorption amount (mmol g^{-1}), P is the equilibrium pressure of the adsorbate in gas phase (mbar), K is equilibrium constant of adsorption, n is the Langmuir-Freundlich coefficient.

Fig. 3 presents a comparison of the experimental data and isotherm equation fit. Table 3 lists the fitting parameters of Langmuir-Freundlich model as well as their correlation coefficients (R^2) for linear regression of *n*-alkanes adsorption data on MIL-101@GO. The high regression coefficients R^2 up to 0.99 indicate that the Langmuir-Freundlich model can well describe the adsorption behaviour of *n*-alkanes on the sample.

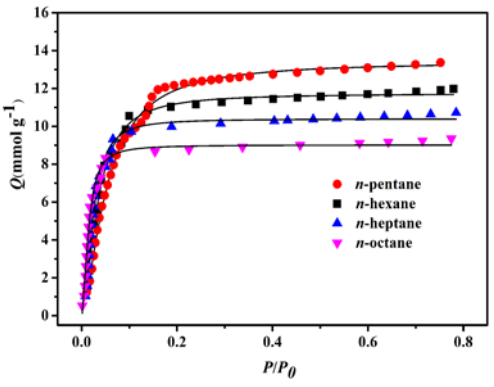

Fig. 3 Langmuir-Freundlich equation fitting of *n*-alkanes adsoption on MIL-101@GO

(points – experimental data; lines – fitting curves)

Table 3 Fitting parameters of Langmuir–Freundlich model for *n*-alkanes adsorption on MIL-101@GO.

n-Alkanes	Langmuir–Freundlich model			
	Q_{max} (mmol g^{-1})	K ($mbar^{-1}$)	n	R^2
n-Pentane	13.43	0.004	0.644	0.997
n-Hexane	11.73	0.040	0.592	0.993
n-Heptane	10.39	0.480	0.508	0.992
n-Octane	9.01	11.16	0.550	0.990

3.2. Desorption activation energies of n-alkanes

TPD experiments were conducted to estimate desorption activation energies of *n*-alkanes on MIL-101@GO, which evaluate how strongly *n*-alkanes are bound to the surfaces of MIL-101@GO. Fig. 4 presents TPD profiles of *n*-alkanes (C5 to C8) on MIL-101@GO. It could be seen that there was an obvious peak in each TPD spectrum due to desorption of the adsorbate from MIL-101@GO. A gradual increase in the heating rate β_H led to an increase in the peak temperature T_p.

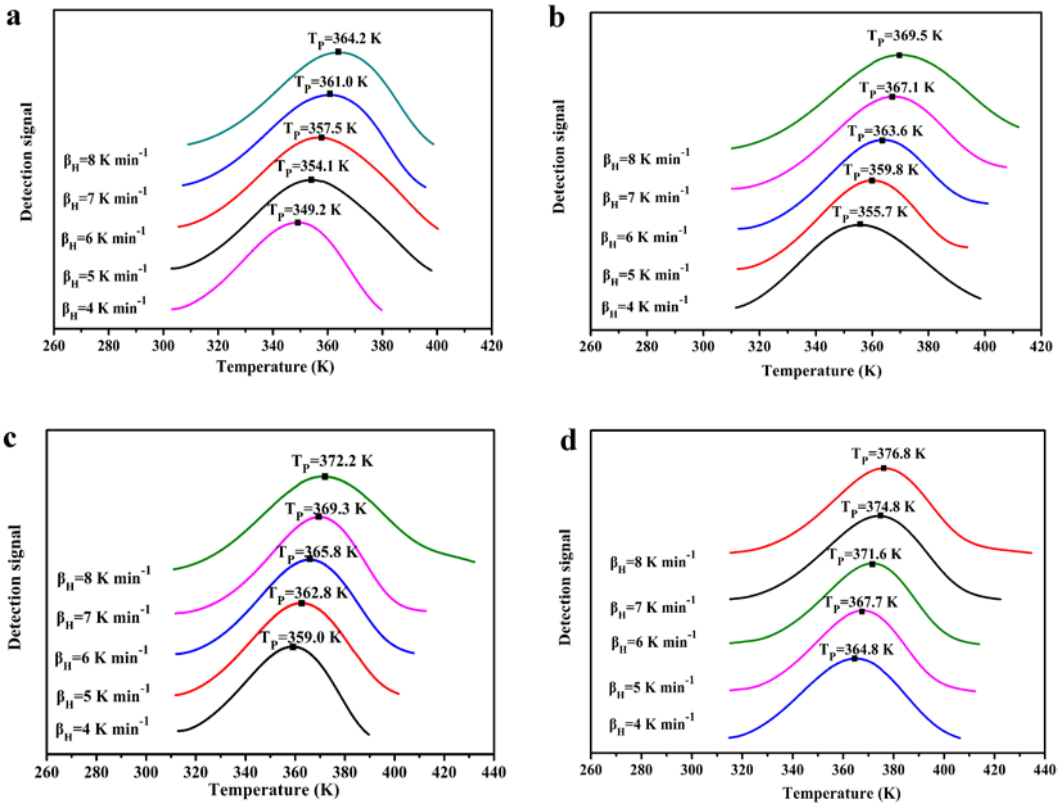

Fig. 4 TPD profiles of *n*-alkanes on MIL-101@GO at different heating rates as follows: (a) *n*-pentane, (b) *n*-hexane, (c) *n*-heptane and (d) *n*-octane.

Knowing a series of T_p at different heating rates, desorption activation energy E_d of *n*-alkanes on

MIL-101@GO can be calculated using the equation[14, 51]

$$\ln\left(\frac{\beta_H}{RT_p^2}\right) = -\left(\frac{E_d}{RT_p}\right) - \ln\left(\frac{E_d}{k_0}\right) \quad (2)$$

where β_H is the heating rate (K min^{-1}), T_p is the peak temperature of TPD curves (K), k_0 is the desorption rate coefficient (s^{-1}), E_d is the desorption activation energy of adsorbate (kJ mol^{-1}) and R is the gas constant(8.314 J K^{-1} mol^{-1}).

Fig. 5 depicts the linear dependences between $\ln[(T_p^2R)/\beta_H]$ and $1/T_p$ for estimation of desorption activation energies of *n*-alkanes on MIL-101@GO. E_d can be found out from the slope E_d/R of the straight line. Table 4 lists the desorption activation energy, E_d, of C5-C8 on MIL-101@GO. It showed that the desorption activation energies of *n*-alkanes increased with the alkyl chain length, which followed the order: C8 > C7 > C6 > C5. It can be attributed to an increase in the interaction between *n*-alkanes and MIL-101@GO when the length of alkyl chain increases.

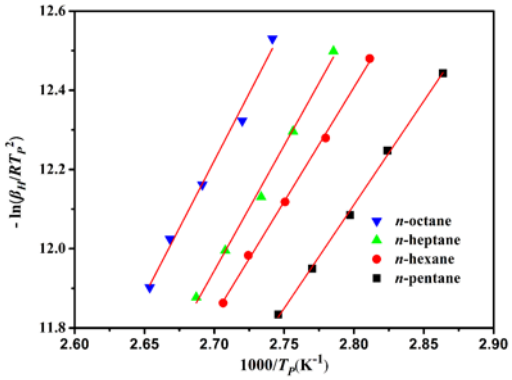

Fig. 5 Linear dependences between $\ln[(T_p^2R)/\beta_H]$ and $1/T_p$ for TPD of the various *n*-alkanes on MIL-101@GO

Table 4 Desorption peak temperatures of *n*-alkanes at different heating rates and desorption activation energies of *n*-alkanes on MIL-101@GO.

n-Alkanes	The peak temperatures T_p at different heating rates (K)					Desorption activation energy E_d(kJ mol^{-1})
	4 K min^{-1}	5 K min^{-1}	6 K min^{-1}	7 K min^{-1}	8 K min^{-1}	
n-Pentane	349.2	354.1	357.5	361.0	364.2	43.49
n-Hexane	355.7	359.8	363.6	367.1	369.5	47.94
n-Heptane	359.0	362.8	365.8	369.3	372.2	52.52
n-Octane	364.8	367.7	371.6	374.8	376.8	56.54

Fig. 6 presents the values of E_d as functions of the number of carbon atoms on the alkyl chains and

polarizability of *n*-alkanes. It was observed linear evolution of the desorption activation energy with the carbon number and polarizability of *n*-alkanes. When *n*-alkane chain was elongated by a single -CH_2- group, its desorption activation energy increased by a constant increment about 4.50 kJ/mol, as shown in Fig.6a. This is also consistent with the trend that an increase in carbon chain length leads to an almost incremental increase in enthalpy of adsorption, which has been previously reported in the case of MIL-53 and MIL-47.[52] In addition, Fig.6b showed that the desorption activation energies of *n*-alkanes on MIL-101@GO was in direct proportion to their polarizability.

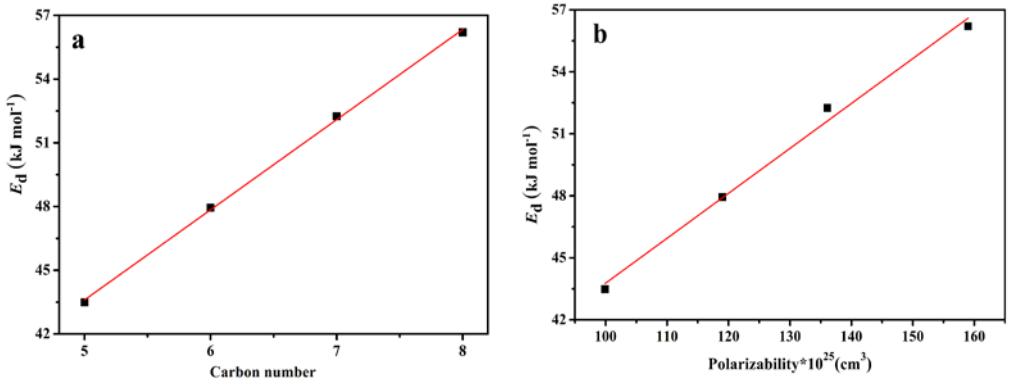

Fig. 6 Desorption activation energies of *n*-alkanes on MIL-101@GO as functions of (a) carbon number and (b) polarizability of the *n*-alkanes

3.3. Cycle Performance of n-alkane adsorption on MIL-101@GO

To examine the reversibility of *n*-alkanes adsorption on composite MIL-101@GO, five consecutive cycles of *n*-alkane adsorption-desorption on the composite were performed at 298 K. *n*-Octane was chosen as probe molecule, since it is not only a model molecule representing a category of *n*-alkanes, but also has strong interaction with MIL-101@GO. After the isotherm measurements of *n*-alkanes on the sample MIL-101@GO, the sample was vacuumed (5 to 10 Pa) at 298 K for 3 h. Then the *n*-octane isotherm was measured at 298 K. After that, the sample was regenerated again, followed by measuring adsorption isotherm of *n*-alkane, which was done for five times. Fig. 7 shows the five isotherms of *n*-octane on MIL-101@GO obtained during five consecutive cycle measuring at 298 K. It was clearly visible that five isotherm curves of *n*-alkane on MIL-101@GO were nearly overlapping, showing robust cycling performance of MIL-101@GO. It suggests that *n*-octane adsorption on MIL-101@GO is reversible.

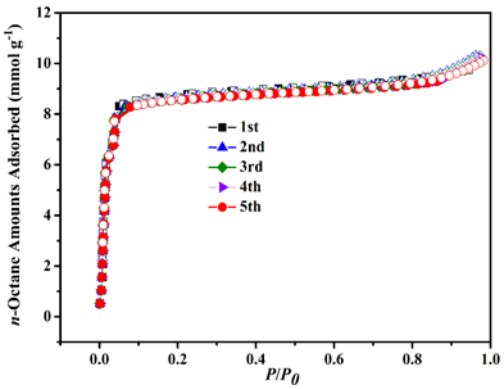

Fig. 7 Cycle performance of *n*-octane adsorption on MIL@GO at 298 K

4. Conclusions

In this work, we present the in depth study of the adsorption behaviour of a series of *n*-alkane vapors on the composite MIL-101@GO. Isotherms of a series of *n*-alkanes on MIL-101@GO were measured. Temperature-programmed desorption (TPD) experiments were conducted to estimate desorption activation energies of *n*-alkanes on MIL-101@GO. The results showed that the adsorption capacities of *n*-alkanes on MIL-101@GO increased with the hydrocarbon chain length at region of low pressure, while the trend was reversed at region of high pressure. The adsorption capacities of *n*-alkanes on MIL-101@GO were about 1.6-11 times higher than those of the conventional activated carbons and the zeolites. The Langmuir–Freundlich model represented the isotherms of *n*-alkanes well. Desorption activation energies of *n*-alkanes on MIL-101@GO increased linearly with the carbon number of *n*-alkanes. Cycle experiments of *n*-octane adsorption-desorption showed the isotherms of *n*-octane in all five cycles were nearly overlapping, suggesting that MIL-101@GO had excellent reversibility of *n*-alkane adsorption. High adsorption capacity and excellent adsorption/desorption performance of *n*-alkane make the composite MIL-101@GO become a promising candidate for industrial applications in field of efficient recovery and removal of gasoline vapor.

Acknowledgments

This work was supported by the National Natural Science Foundation of China (Nos. 21276092 and 20936001), the Science and Technology Research Foundation of Guangzhou City (No. 200910814001), the State Key Lab of Subtropical Building Science (Grant C714004z), and the Fundamental Research Funds for the Central Universities.

Notes and references

1 L. Jia, W. Yu, C. Long and A. Li, *Environ. Sci. Pollut. R.*, 2014, **21**, 3756-3763.
2 Y. K. Ryu, J. W. Chang, S. Y. Jung and C. H. Lee, *J. Chem. Eng. Data*, 2002, **47**, 363-366.
3 K. Chue, Y. K. Park and J. K. Jeon, *Korean J. Chem. Eng.*, 2004, **21**, 676-679.

4 W. Huang, J. Bai, S. Zhao and A. Lv, *J. Loss Prevent. Proc.*, 2011, **24**, 178-186.

5 M. A. Mehlman, *Environ. Res.*, 1992, **59**, 238-249.

6 I. I. El-Sharkawy, H. J. Ming, K. C. Ng, C. Yap and B. B. Saha, *J. Chem. Eng. Data*, 2007, **53**, 41-47.

7 Y. Liu, X. Feng and D. Lawless, *J. Membrane Sci.*, 2006, **271**, 114-124.

8 J. L. Shie, C. Y. Lu, C. Y. Chang, C. Y. Chiu, D. J. Lee, S. P. Liu and C. T. Chang, *J. Chin. Inst. Chem. Eng.*, 2003, **34**, 605-616.

9 F. Xu, S. Xian, Q. Xia, Y. Li and Z. Li, *Adsorpt. Sci. Technol.*, 2013, **31**, 325-340.

10 Z. R. Herm, E. D. Bloch and J. R. Long, *Chem. Mater.*, 2013, **26**, 323-338.

11 Y. K. Ryu, H. J. Lee, H. K. Yoo and C. H. Lee, *J. Chem. Eng. Data*, 2002, **47**, 1222-1225.

12 A. Möller, A. Pessoa Guimaraes, R. Gläser and R. Staudt, *Micropor. Mesopor. Mat.*, 2009, **125**, 23-29.

13 Z. Zhang, S. Xian, Q. Xia, H. Wang, Z. Li and J. Li, *AIChE J.*, 2013, **59**, 2195-2206.

14 Z. Zhang, S. Huang, S. Xian, H. Xi and Z. Li, *Energ. Fuel.*, 2011, **25**, 835-842.

15 Z. Zhao, X. Ma, Z. Li and Y. Lin, *J. Membrane Sci.*, 2011, **382**, 82-90.

16 K. Li, D. H. Olson, J. Y. Lee, W. Bi, K. Wu, T. Yuen, Q. Xu and J. Li, *Adv. Funct. Mater.*, 2008, **18**, 2205-2214.

17 H. Wu, Q. Gong, D. H. Olson and J. Li, *Chem. Rev.*, 2012, **112**, 836.

18 L. Wu, J. Xiao, Y. Wu, S. Xian, G. Miao, H. Wang and Z. Li, *Langmuir*, 2014, **30**, 1080 − 1088.

19 Y. Wu, J. Xiao, L. Wu, C. Ma, H. Xi, Z. Li and H.Wang, *J. Phys. Chem. C*, 2014,**118**,22533-22543.

20 Z. Zhao, X. Li, S. Huang, Q. Xia and Z. Li, *Ind. Eng. Chem. Res.*, 2011, **50**, 2254-2261.

21 Z. Zhao, X. Li and Z. Li, *Chem. Eng. J.*, 2011, **173**, 150-157.

22 J. Shi, Z. Zhao, Q. Xia, Y. Li and Z. Li, *J. Chem. Eng. Data*, 2011, **56**, 3419-3425.

23 M. T. Luebbers, T. J. Wu, L. J. Shen and R. I. Masel, *Langmuir*, 2010, **26**, 15625-15633.

24 T. K. Trung, I. Deroche, A. Rivera, Q. Yang, P. Yot, N. Ramsahye, S. D. Vinot, T. Devic, P. Horcajada and C. Serre, *Micropor. Mesopor. Mat.*, 2011, **140**, 114-119.

25 I. Deroche, S. Rives, T. Trung, Q. Yang, A. Ghoufi, N. A. Ramsahye, P. Trens, F. Fajula, T. Devic, C. Serre, G. Ferey, H. Jobic and G. Maurin, *J. Phys. Chem. C*, 2011, **115**, 13868-13876.

26 T. K. Trung, N. A. Ramsahye, P. Trens, N. Tanchoux, C. Serre, F. Fajula and G. Férey, *Micropor. Mesopor. Mat.*, 2010, **134**, 134-140.

27 T. K. Trung, P. Trens, N. Tanchoux, S. Bourrelly, P. L. Llewellyn, S. Loera-Serna, C. Serre, T. Loiseau, F. Fajula and G. Férey, *J Am. Chem. Soc.*, 2008, **130**, 16926-16932.

28 N. A. Ramsahye, T. K. Trung, L. Scott, F. Nouar, T. Devic, P. Horcajada, E. Magnier, O. David, C. Serre and P. Trens, *Chem. Mater.*, 2013, **25**, 479-488.

29 C. Y. Huang, M. Song, Z. Y. Gu, H. F Wang and X.P. Yan, *Environ. Sci. Technol.*, 2011, **45**, 4490-4496.

30 C. Petit and T. J. Bandosz, *Adv. Mater.*, 2009, **21**, 4753-4757.

31 C. Petit, B. Levasseur, B. Mendoza and T. J. Bandosz, *Micropor. Mesopor. Mat.*, 2012, **154**, 107-112.

32 Y. Zhao, M. Seredych, Q. Zhong and T. J. Bandosz, *RSC Adv.*, 2013, **3**, 9932-9941.

33 C. Petit and T. J. Bandosz, *Dalton T.*, 2012, **41**, 4027-4035.

34 R. Kumar, K. Jayaramulu, T. K. Maji and C. N. R. Rao, *Chem. Commun.*, 2013, **49**, 4947-4949.

35 G. Férey, C. Mellot-Draznieks, C. Serre, F. Millange, J. Dutour, S. Surblé and I. Margiolaki, *Science*, 2005, **309**, 2040-2042.

36 G. Chang, Z. Bao, Q. Ren, S. Deng, Z. Zhang, B. Su, H. Xing and Y. Yang, *RSC Adv.*, 2014, **4**, 20230-20233.

37 X. Q. Liu, H. Zhou, Y. Zhang, Y. J. Liu and A. H. Yuan, *Chinese J. Chem.*, 2012, **30**, 2563-2566.

38 I. Ahmed, N. A. Khan and S. H. Jhung, *Inorg. Chem.*, 2013, **52**, 14155-14161.

39 X. Zhou, W. Huang, J. Shi, Z. Zhao, Q. Xia, Y. Li, H. Wang and Z. Li, *J. Mater. Chem. A*, 2014, **2**, 4722-4730.

40 X. J. Sun, Q. B. Xia, Z. X. Zhao, Y. W. Li and Z. Li, *Chem. Eng. J.*, 2014, **239**, 226-232.

41 J. R. Li, R. J. Kuppler and H. C. Zhou, *Chem. Soc. Rev.*, 2009, **38**, 1477-1504.
42 M. J. Gray, R. C. Mebane, H. N. Womack and T. R. Rybolt, *J. Colloid Interf. Sci*., 1995, **170**, 98-101.
43 C. E. Webster, R. S. Drago and M. C. Zerner, *J. Am. Chem. Soc.*, 1998, **120**, 5509-5516.
44 P. Trens, H. Belarbi, C. Shepherd, P. Gonzalez, N. A. Ramsahye, U. H. Lee, Y. K. Seo and J. S. Chang, *Micropor. Mesopor. Mat.*, 2014, **183**, 17-22.
45 P. A. Russo, M. Carrott and P. J. M. Carrott, *New J. Chem.*, 2011, **35**, 407-416.
46 X. Zhao, Q. Ma and G. Lu, *Energ. fuel*., 1998, **12**, 1051-1054.
47 M. Hartmann and C. Bischof, *J. Phys. Chem. B*, 1999, **103**, 6230-6235.
48 Q. L. Huang, H. Vinh-Thang, A. Malekian, M. Eic, D. Trong-On and S. Kaliaguine, *Micropor. Mesopor. Mat.*, 2006, **87**, 224-234.
49 A. J. Fletcher, Y. Yuzak and K. M. Thomas, *Carbon*, 2006, **44**, 989-1004.
50 Z. P. Liu, W. M. Fan, J. H. Ma and R. F. Li, *Adsorption*, 2012, **18**, 493-501.
51 Q. B. Xia, Z. Li, L. M. Xiao, Z. J. Zhang and H. X. Xi, *J. Hazard. Mater.*, 2010, **179**, 790-794.
52 N. Rosenbach Jr, A. Ghoufi, I. Deroche, P. L. Llewellyn, T. Devic, S. Bourrelly, C. Serre, G. Ferey and G. Maurin, *Phys. Chem. Chem. Phys.*, 2010, **12**, 6428-6437.